Please do not adjust margins

Dalton Transactions

ARTICLE

Silica@Layered Double Hydroxide Core-shell Hybrid Materials

Wing L. J. Kwok, Dana-Georgiana Crivoi, Chunping Chen, Jean-Charles Buffet and Dermot O'Hare*

Received 00th January 20xx,
Accepted 00th January 20xx

DOI: 10.1039/x0xx00000x

www.rsc.org/

A series of silica@layered double hydroxides (SiO_2@Mg_2Al-CO_3-AMO-LDHs) have been synthesised by *in-situ* precipitation of Mg_2Al-CO_3-LDH at room temperature in the presence of amorphous spherical silica particles (~500 nm). We have systematically investigated a number of synthetic parameters in order to evaluate their effects on the composition, morphological and physical properties of the isolated materials. Syntheses carried out at moderate stirring speeds (*e.g.* 500 rpm) were found to promote the formation of vertically aligned LDH platelets with respect to the silica surface. Addition rates of the metal solutions, slower than 0.43 mmol h^{-1}, were found to create a thicker LDH shell consisting of vertically aligned LDH platelets. When the metal solutions were added rapidly (0.86 mmol h^{-1}), we observed that for both slow and fast stirring speeds the synthesised core-shell materials had thin LDH shells and the majority of the LDH precipitated independent of the silica, forming unbound "free" LDH.

Introduction

Inorganic nanoparticles have attracted increasing attention in recent years from a variety of scientific fields including drug delivery,[1-3] electronics[4-6] and catalysis.[7-11] Layered double hydroxide-based compounds are one such class of materials which are being extensively explored for applications in these areas. Layered double hydroxides (LDHs) constitute a class of inorganic compounds with a general formula $[M_{1-x}M_x'(OH)_2]^{y+}[A_{y/n}^{n-}]\cdot aH_2O$, where M and M′ are typically metal di- and trications, respectively, $0 < x < 1$, and A an interlayer anion with charge n.[12] In LDHs, partial substitution of divalent cations in the layers by trivalent cations results in a net positive charge on the layers so anions occupy the interlayer region in order to maintain charge neutrality.[13] The anions range from simple (*e.g.* chloride, hydroxide, and carbonate) to large surfactants and proteins.[14-17] Owing to their flexibility in composition and echangeable interlayer anions, LDHs have found application in drug delivery,[1,18-20] waste water treatment,[21-24] Michael addition,[11,25] oxidation,[26-28] and transesterification.[29-31]

An important characteristic of LDHs is the dispersion of metal cations in the layers. As such, LDH-derived catalyst precursors, with a few well-documented exceptions,[32,33] contain a homogeneous distribution of metal cations that can be subsequently calcined and reduced to obtain stable and highly dispersed metal nanoparticles on the surface of an amorphous support.[34,35] The uniform dispersion of metal cations or anions within the layers also makes LDHs good candidates for supercapacitor electrode materials.[4,6,36-38]

Thermal treatment of LDHs yields mixed metal oxides (MMOs), also referred to as layered double oxides (LDOs), which have a unique "memory effect" feature.[39] The composition of an LDO depends on the calcination temperature and consequently an LDO may contain amorphous as well as crystalline phases.[40,41] It is found that LDHs calcined below a certain temperature can be reconstructed into their original layered structure by rehydration,[39] adsorption of anions,[42] or simply exposure to air.[13] The "memory effect" is a valuable feature of LDHs as it can be used to intercalate functional inorganic and organic anions into LDHs galleries, and so can enable syntheses of materials that are otherwise difficult to prepare by any other method.[43]

Recently, O'Hare and co-workers developed a post-synthesis method to obtain LDHs with high BET areas, large pore volume and good dispersibility in non-polar solvents.[44,45] The aqueous miscible organic solvent treatment (AMOST) involves the dispersion of a wet LDH cake in an organic medium such as acetone or ethanol. The so-called AMO-LDHs have a general formula $[M_{1-x}M_x'(OH)_2]^{y+}[A_{y/n}^{n-}]\cdot aH_2O\cdot b$(AMO-solvent).[45] AMO-solvent molecules replace water molecules on the surface weakening the strong hydrogen bonding interactions that bind the anions and layers in a rigid stacked structure.[45] The loss of surface bound water molecules also changes the LDH from hydrophilic to organophilic so AMO-LDHs are highly dispersible in non-polar hydrocarbon solvents.[46]

The growth of LDH platelets vertically on a nano-support is another strategy to avoid *ab*-face aggregation. A variety of core materials have been explored to date including SiO_2,[47,48] TiO_2,[49] Fe_3O_4,[50-52] and carbon.[36,53,54] Direct deposition, sol-gel, and co-precipitation are three commonly employed methods of core@LDH synthesis.[55] Direct deposition involves the combination of LDH nanoparticles and the core material after their separate syntheses. Li *et al.* used this self-assembly

Chemistry Research Laboratory, University of Oxford, 12 Mansfield Road, Oxford, OX1 3TA, UK. Email: dermot.ohare@chem.ox.ac.uk

Electronic Supplementary Information (ESI) available: [FTIR, PXRD, SEM, SEM-EDS, TEM, TGA and BET]. See DOI: 10.1039/x0xx00000x

Please do not adjust margins

Please do not adjust margins

method to create magnetic supraparticles@LDH nanocomposites for biomedical applications and found that the post-ageing temperature has a significant effect on the structure and physicochemical properties of the nanocomposites.[56] In the sol-gel method, the core material is immersed in an AlOOH primer solution, agitated for hours, separated, washed and dried. This cycle is repeated several times.[37,57] The AlOOH coating acts as a source of aluminium which allows for crystallisation of an LDH shell to take place on the surface. Shao *et al.* reported the use of a sol-gel technique in the synthesis of Fe_3O_4@SiO_2@NiAl-LDH microspheres which were used to selectivity adsorb a His-tagged protein from an *E.coli lysate*.[58]

Co-precipitation is an easier method for preparing core@LDHs hybrids, which typically involves the adsorption of metal cations onto the surface of the core followed by crystal growth on the core by the addition of a precipitating agent such as a base.[19] Growth of the LDH shell is facilitated by ageing and/or hydrothermal treatment.[51] Ultrasound treatment has also been applied to assist the dispersion of metal cations on the surface of the core material, allowing for homogeneous growth of the LDH.[23] To date, the effect of pH and temperature on the morphology of SiO_2@LDH synthesised by *in-situ* co-precipitation has been reported by Chen *et al*.[48] They found that high pH and temperatures caused dissolution of the silica core, leading to yolk- and hollow-shell nanocomposites (Fig. 1).

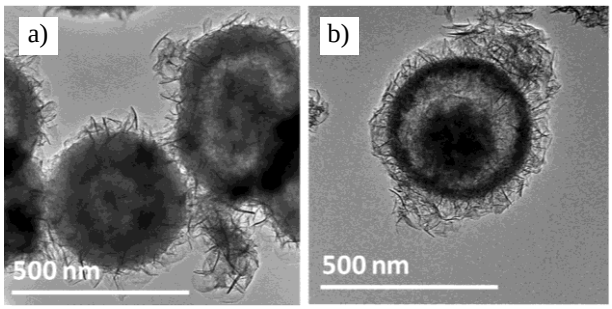

Fig. 1 TEM images of (a) hollow-shell and (b) yolk-shell SiO_2@Mg_2Al-LDH obtained from Chen *et al.*.[48]

Herein, we present how the *in-situ* co-precipitation conditions may influence the growth, structure and composition of the LDH shell on the silica substrate.

Results and discussion

Core-shell SiO_2@Mg_2Al-CO_3-AMO-LDHs (Mg_2Al-CO_3 = $[Mg_{0.67}Al_{0.33}(OH)_2][CO_3]_{0.17}$) were prepared by *in-situ* precipitation of Mg_2Al-CO_3-LDH at room temperature in the presence of amorphous spherical silica particles (~500 nm). The *in-situ* precipitation was initiated by addition of a solution of $Mg(NO_3)_2.6H_2O$ and $Al(NO_3)_3.9H_2O$ (Mg/Al molar ratio 2:1) to an aqueous suspension of the silica particles and Na_2CO_3 while maintaining the mixture at pH 10. The rate of addition of the mixed metal solution was varied between 0.11 – 0.86 mmol h^{-1} and the suspension was stirred at various speeds (between 0 – 1000 rpm) at fixed solution volume and reactor size. We defined 500 rpm as a moderate stirring speed and thus stirring speeds less than 500 rpm are defined as slow, whilst those above 500 rpm are fast. AMO treatment was performed on the SiO_2@LDH wet-cake using ethanol. The analytical data suggests the chemical composition of these materials is in the range SiO_2@$[[Mg_{0.67}Al_{0.33}(OH)_2(CO_3)_{0.17}]\cdot a(H_2O)\cdot b(EtOH)]_{0.59\text{-}0.66}$, where $0.21 \leqslant a \geqslant 0.30$ and $0.12 \leqslant b \geqslant 0.18$ (Table S1).

Variation of stirring speed

Fig. 2 and S1 compare the FTIR spectra of SiO_2@Mg_2Al-CO_3-AMO-LDHs synthesised using a range of stirring speeds at two different metal addition rates. The absorption band at *ca.* 1100 cm^{-1} is due to the Si-O stretching mode of the silica core and the remaining features are characteristic of the LDH phase: the broad band between 3000 – 3500 cm^{-1} is due to the stretching vibration of metal-bound hydroxyl groups (M-O-H); the ν_3 anti-symmetric stretching mode of interlayer carbonate anions give rise to the band at *ca.* 1360 cm^{-1}; and the bending mode of water occurs at *ca.* 1650 cm^{-1}.

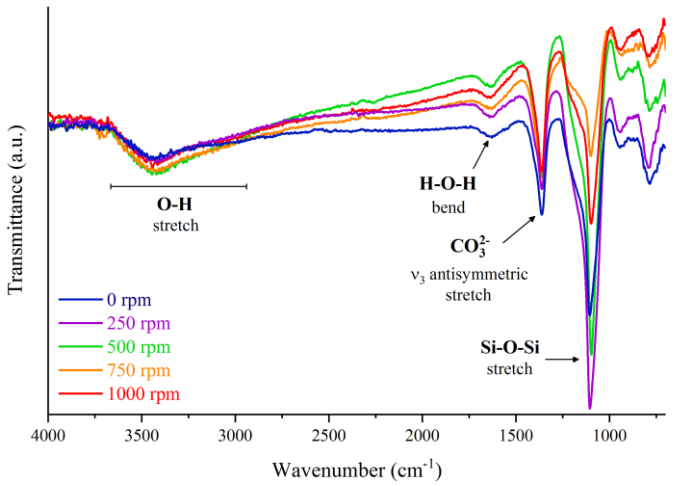

Fig. 2 FTIR spectra of SiO_2@Mg_2Al-CO_3-AMO-LDHs synthesised at stirring speed 0 – 1000 rpm at a metal addition rate of 0.11 mmol h^{-1}.

Powder X-ray diffractograms have been recorded for SiO_2@Mg_2Al-CO_3-AMO-LDHs synthesised with different stirring speeds (Fig. 3) and at two different metal addition rates (Fig. S2). All samples show a series of characteristic Bragg reflections that may be indexed to the unit cell (a = *b* = 3.039 Å; *c* = 22.83 Å) corresponding to Mg_2Al-CO_3-LDH. These Bragg reflections are superimposed upon a broad feature between *ca.* 2θ = 15 – 30° due to the amorphous silica core scattering. We observe a small change in the relative peak intensities of these two phases between different synthetic procedures. The sample prepared at 500 rpm shows a greater proportion of LDH scattering relative to the silica background. However, XRD cannot determine if this entire LDH X-ray scattering is due to silica-bound LDH.

This journal is © The Royal Society of Chemistry 20xx

Please do not adjust margins

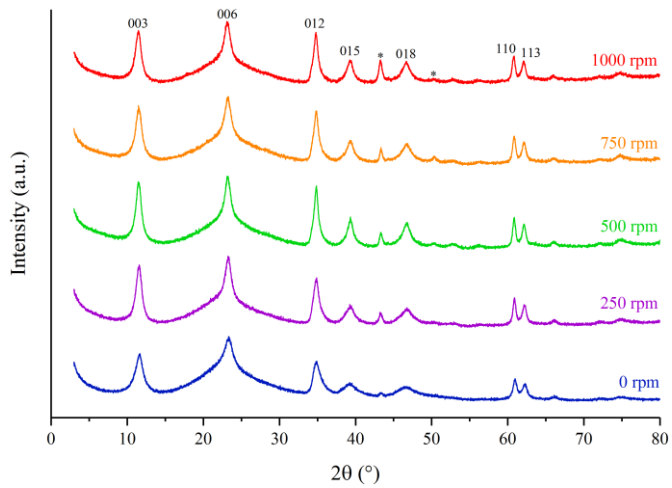

Fig. 3 Powder XRD diffractograms of SiO_2@Mg_2Al-CO_3-AMO-LDHs synthesised with stirring rates of 0 – 1000 rpm at a metal addition rate of 0.11 mmol h^{-1}. *Reflections due to the sample holder.

A qualitative assessment of the amount of free LDH can be made from electron microscopy images, SEM and SEM-EDS, (Figs. S3 – S6). The presence of free LDH is greatest in the samples synthesised with stirring speeds 0 (*i.e.* no stirring) and high speeds (750 and 1000 rpm). For the reaction without stirring, the silica particles sunk to the bottom of the vessel and, therefore, had limited contact with the incoming metal solution, leading to non-uniform LDH growth on the silica particles and precipitation of LDH in a silica-depleted solution. The growth of LDH was also diffusion limited under these conditions. For 750 and 1000 rpm (*i.e.* the highest stirring speeds) we believe the free LDH is due to strong shearing forces exerted on the particles suspended in solution which consequently leads to LDH nucleating in solution rather than on the silica particle surface. In comparison, at lower stirring speeds, the metal cations have a greater probability of being in the vicinity of a silica particle. The TEM images also show that larger LDH particles (LDH shell thicknesses) are formed under low stirring speeds (*e.g.* 500 rpm), (Fig. S6). This is because the shear forces at these speeds are weaker and therefore less likely to pull existing particles apart, thus allowing the LDH platelets to grow larger under Ostwald ripening. These observations are supported by the crystallite sizes calculated using the Scherrer equation and (110) diffraction peaks (Table S2).

The relative orientation of the LDH platelets with respect to the silica surface is mixed but there is a tendency for vertically oriented platelets at lower stirring speeds (Fig. S6c) and horizontal platelets at higher stirring speeds (Fig. S6d and S6e). This can be explained in terms of the abundance of LDH nuclei on the surface of the silica cores. When the LDH nuclei are densely packed on the silica surface, competition for space means that the dominant direction of platelet growth is perpendicular to the surface (*i.e.* vertical).

N_2 BET areas of SiO_2@Mg_2Al-CO_3-AMO-LDHs were measured and show a peak for the sample synthesised using a stirring speed of 500 rpm (Fig. S7a and Table S3). This is in agreement with the TEM images shown in Fig. S6, which reveal that this is the optimum stirring speed for achieving large, vertically-oriented platelets that create an open honeycomb-like LDH shell. As stirring speed increases, fewer inter-platelet voids are created because the abundance of LDH nuclei on the silica surface is low and vertical growth is less favourable. The pore size distribution (computed using the BJH desorption method, Fig. S7c) shows that these voids are in the mesoporous size range, with the lower stirring speeds generally having a greater number of larger pores.

Solid state ^{27}Al NMR has been recorded for the SiO_2@Mg_2Al-CO_3-AMO-LDHs (Fig 4). In pure LDH phases, aluminium occupies only octahedral (O_h) sites within the metal hydroxide layers, while in these hybrid materials a small population of tetrahedrally coordinated Al^{3+} (T_d) was observed; we have assigned these to Al^{3+} sites bridging to the silica surface forming Si-O-Al bonds.[48] The ratio of Al^{3+} in T_d and O_h environments may be obtained from the integration of the solid state ^{27}Al NMR spectra and provides a more quantitative analysis of the degree of LDH coverage on the silica surface. The integrated intensity of the T_d : O_h ^{27}Al resonances changes from 1:8 to 1:11 between sample prepared at 500 rpm compared to 750 rpm (Table S4). A greater proportion of T_d environments in the sample prepared at a stirring speed of 500 rpm suggests a higher level of LDH coverage on the silica surface.

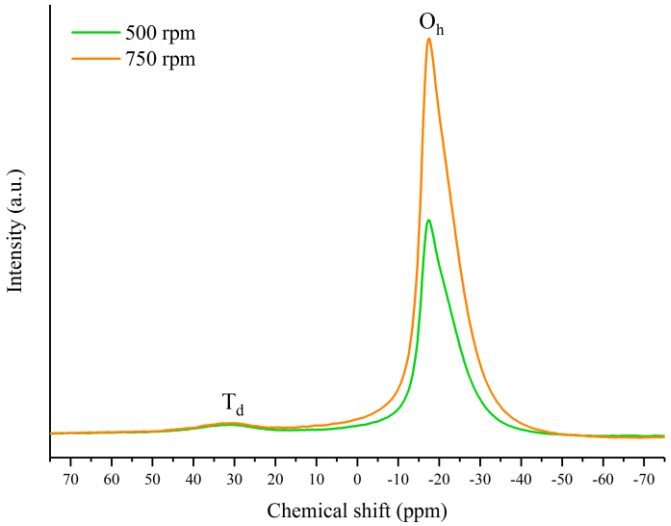

Fig. 4 Solid state ^{27}Al DPMAS NMR spectra of SiO_2@Mg_2Al-CO_3-AMO-LDHs synthesised with a stirring speeds of 500 and 750 rpm at a fixed metal addition rate of 0.43 mmol h^{-1}.

Variation of metal addition rate

Different batches of SiO_2@Mg_2Al-CO_3-AMO-LDHs have been prepared at a fixed stirring speed but at different metal salt addition rate. Figs. 5 and S8 compare the powder X-ray diffractograms of SiO_2@Mg_2Al-CO_3-AMO-LDHs samples prepared using stirring speeds of 500and 1000 rpm, respectively. All samples show the characteristic diffractions for Mg_2Al-CO_3-AMO-LDH superimposed upon broad silica scattering feature. However, we also observe a change in the peak widths of diffractions associated with the LDH, suggesting

Please do not adjust margins

that the LDH crystallite size of the silica-grafted LDH plates is influenced by the metal salt addition rate.

The LDH crystallite size for each sample was determined by application of the Scherrer equation. Fig. S9 summarises the crystallite sizes as a function of (i) stirring speed and (ii) metal addition rate. Both parameters do have a significant effect on the crystallite size.

The line widths of the Bragg diffraction peaks assigned to the LDH phase were broadest for samples synthesised with the highest metal addition rates (0.43 and 0.86 mmol h^{-1}). TheFTIR spectra (Fig. S10) of these two samples also show the weakest carbonate absorption intensity (v_3 antisymmetric stretch at *ca.* 1360 cm^{-1}) suggesting that these batches have the lowest degree of LDH incorporation (*i.e.* the thinnest LDH shells).

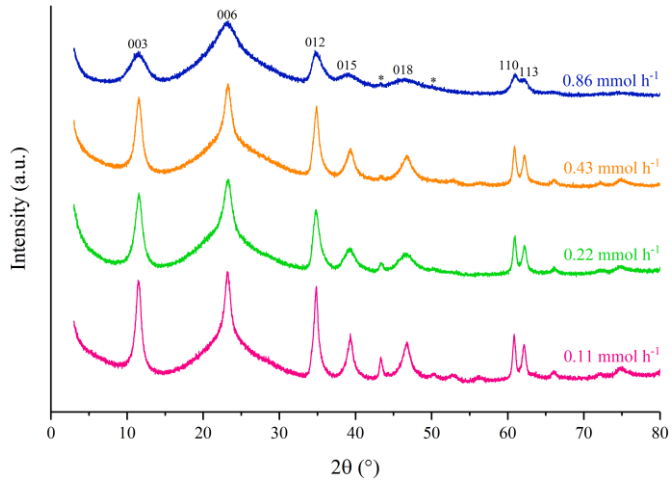

Fig. 5 Powder XRD diffractograms of SiO_2@Mg_2Al-CO_3-AMO-LDHs synthesised a three different additions rates at a fixed stirring speed of 500 rpm. *Reflections due to the sample holder.

The TEM images support the XRD and FTIR results, showing smaller crystallites and thinner LDH shells for the SiO_2@Mg_2Al-CO_3-AMO-LDHs synthesised at the highest metal addition rates (Figs. 6 and S11). In addition, these samples also have poorer coverage and greater amounts of free LDH. These results can be rationalised by taking into account the ageing process: with slower metal addition rates the LDH platelets have more time to grow – the addition time being greater for the same volume of solution – so they undergo a longer period of Ostwald ripening. Thus, the LDH crystallites are larger and the overall shell thickness on the silica cores thicker. In comparison, at high metal addition rates, nucleation sites form rapidly as a result of the high metal ion concentration. The LDH platelets also appear to be predominantly vertical with respect to the silica surface. This is due to the conditions of higher saturation generating a large number of nuclei that become compactly packed on the surface so the (110) plane is more accessible to incoming cations than the (003).

Table S5 summarises the BET areas of SiO_2@Mg_2Al-CO_3-AMO-LDHs synthesised with different metal addition rates. It can be seen that, for a given stirring speed, the BET area is approximately constant and that the stirring speed has a greater impact on the BET area.

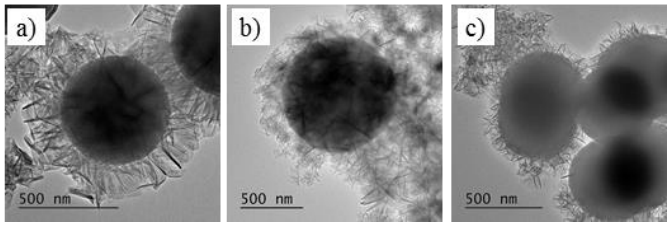

Fig. 6 TEM images of SiO_2@Mg_2Al-CO_3-AMO-LDHs synthesised with metal addition rates of a) 0.22, b) 0.43, and c) 0.86 mmol h^{-1} at a fixed stirring speed of 750 rpm.

Thermal stability of SiO_2@Mg_2Al-CO_3-AMO-LDHs

It is known that calcined LDHs, layered double oxides (LDOs), are useful intermediates for functionalised LDHs and that their tuneable acid/base properties can be utilised in catalytic applications. Herein, we are interested in studying the thermal stability of SiO_2@Mg_2Al-CO_3-AMO-LDHs using TGA, FTIR, XRD and TEM. The TGA curves of SiO_2@Mg_2Al-CO_3-AMO-LDH synthesised using different conditions are shown in Fig 7. All the samples show a similar thermal behaviour of endothermic events corresponding to (i) loss of ethanol (AMO-solvent), (ii) loss of interlayer water, (iii) and (iv) dehydroxylation and decarboxylation of the LDH layers.

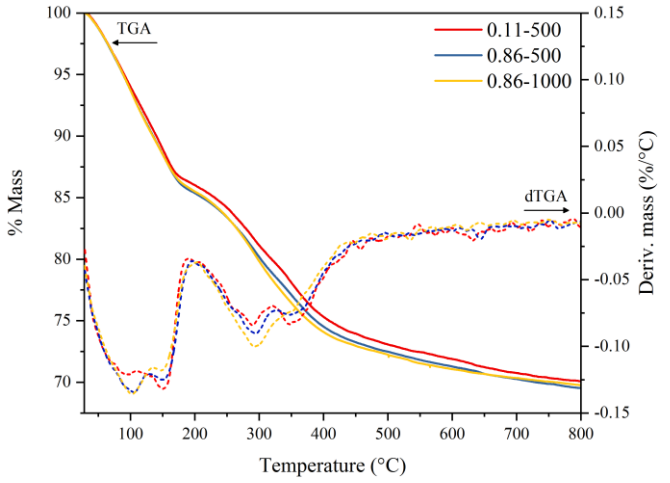

Fig. 7 TGA and dTGA curves for SiO_2@Mg_2Al-CO_3-AMO-LDH. Sample names: *e.g.* "0.11-500" refers to a SiO_2@Mg_2Al-CO_3-AMO-LDH synthesised with a metal addition rate of 0.11 mmol h^{-1} and stirring speed of 500 rpm.

The FTIR spectra of SiO_2@Mg_2Al-CO_3-AMO-LDH calcined up to 700 °C show significant differences to that of the parent SiO_2@LDH (Fig. S12). The disappearance of the broad feature between *ca.* 3000 – 3500 cm^{-1} is due to dehydration and dehydroxylation. Interlayer water and carbonate are also eliminated so the bands at *ca.* 1600 and 1360 cm^{-1} are absent. Sharp absorptions below 1000 cm^{-1} are due to the formation of M-O-M (M = Mg^{2+}, Al^{3+}) bridges between adjacent layers following the collapse of the layered structure upon the loss of interlayer species.

The XRD data indicate the presence of a periclase MgO phase in the samples calcined above 350°C (Fig. 9). The broadness of the Bragg reflections assigned to the MgO indicates a small

This journal is © The Royal Society of Chemistry 20xx

Please do not adjust margins

crystallite size. Furthermore, the lattice parameter of the MgO phase ($a = b = c = 4.18$ Å) is smaller than that of pure MgO (4.21 Å),[59] indicating some incorporation of Al^{3+} in the structure. It is interesting to observe the Bragg reflection at $2\theta = 35.1°$ that may be ascribed to the presence of $Mg_3Al_2(SiO_4)_3$ in the sample after thermal treatment. We believe this is formed by the reaction of silica with MgO and AlO_x during decomposition of the LDH. The MgO Bragg reflections, and those corresponding to $Mg_3Al_2(SiO_4)_3$, sharpen with increasing calcination temperature, indicating an increase in crystallinity.

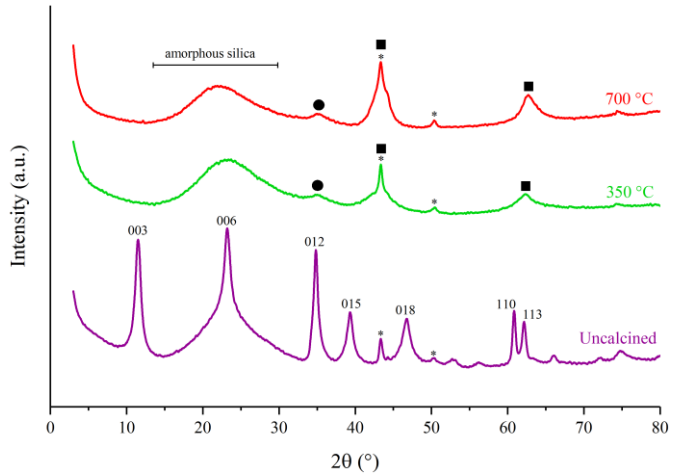

Fig. 9 Powder XRD diffractograms of SiO_2@Mg_2Al-CO_3-AMO-LDH synthesised with metal addition rate 0.11 mmol h^{-1} and 500 rpm, and its calcined products. *Reflections due to the sample holder. Diffraction peaks due to MgO are labelled with a square (■) and those due to $Mg_3Al_2(SiO_4)_3$ with a circle (●).

The TEM images reveal no apparent changes in the silica core upon thermal treatment but the platelets become increasingly "spotty" which suggests that the structure of the LDO is more porous than the parent LDH (Fig. S13). This is the result of the transformation of the hydroxide to oxide: dehydroxylation and decarboxylation occurs between *ca.* 200 – 700 °C and the layered structure collapses upon cation migration to form a mixed metal oxide.

Experimental

General synthesis procedure for core-shell SiO_2@Mg_2Al-CO_3-AMO-LDHs

Core-shell SiO_2@Mg_2Al-CO_3-AMO-LDHs were prepared following a modified literature method.[48] Silica (SiO_2, diameter ~500 nm, 100 mg) was dispersed in deionised water (20 mL) using ultra-sonication for 25 minutes. Sodium carbonate (Na_2CO_3, 0.96 mmol) was then added to the solution and a further 5 minutes of sonication was carried out to form solution A. The pH of solution A was adjusted to pH 10 using a 10 wt% nitric acid solution. Separately, magnesium nitrate hexahydrate ($Mg(NO_3)_2.6H_2O$, 0.96 mmol) and aluminium nitrate nonahydrate ($Al(NO_3)_3.9H_2O$, 0.48 mmol) were dissolved in D.I. H_2O (20 mL) to form solution B. Solution B was added to solution A at room temperature at various rates (15, 30, 60, or 120 mL h^{-1} equivalent to 0.11, 0.22, 0.43 and 0.86 mmol h^{-1}, respectively) and the suspension was stirred at various speeds (0, 250, 500, 750, or 1000 rpm). The pH of the reaction solution was maintained at pH 10 by addition of 1 M NaOH. After the addition of solution B to solution A was completed, the suspension was aged at room temperature with stirring for 1 h. The solid was collected by centrifugation (6000 rpm, 5 minutes) and re-dispersed in D.I. H_2O (40 mL) for 10 minutes. The solid was isolated by centrifugation and washed with D.I. H_2O until the supernatant pH decreased to pH 7. The wet solid was then washed with ethanol (40 mL) and re-dispersed in ethanol (40 mL) for 1 h. The solid was collected by centrifugation and dried under vacuum overnight.

Conclusions

A series of SiO_2@Mg_2Al-CO_3-AMO-LDHs have been synthesised and fully characterised. Batch syntheses using slow stirring speeds were found to promote the formation of vertically aligned LDH platelets with respect to the silica surface. Slow metal addition rates during *in-situ* co-precipitation led to thicker LDH shells of vertically aligned platelets. The samples exhibited N_2 BET areas up to *ca.* 100 m^2 g^{-1}, the highest BET area was observed for samples obtained at a moderate stirring speed (500 rpm).

The experiments indicate that preparing high quality core@LDH needs detailed attention to the synthesis conditions. We found that for core-shell SiO_2@Mg_2Al-CO_3-AMO-LDH materials the use of moderate stirring speeds and slow metal addition rates produced samples with an optimal honeycomb-like morphology and the highest BET area.

The fine crystallisation of LDH particles by their growth onto a support is recognised as a general method to improve catalytic properties by avoiding ab-face aggregation, excess growth of the active species and balance the final basicity and acidity. Studies regarding the catalytic activity of these materials are ongoing and will soon be reported.

Conflicts of interest

The authors declare no conflicts of interest.

Acknowledgements

W.L.J.K., D.-G.C., C.C. and J.-C.B. thank SCG Chemicals Co., Ltd (Thailand) for funding. Dr Nicholas H. Rees (University of Oxford) is thanked for solid state NMR spectroscopy.

Notes and references

1. B. Li, J. He, D. G. Evans and X. Duan, *Appl. Clay Sci.*, 2004, **27**, 199.
2. M. del Arco, S. Gutiérrez, C. Martín, V. Rives and J. Rocha, *J. Solid State Chem.*, 2004, **177**, 3954.
3. S. Guan, R. Liang, C. Li, D. Yan, M. Wei, D. G. Evans and X. Duan, *J. Mater. Chem. B*, 2016, **4**, 1331.

Please do not adjust margins

4. Z.-A. Hu, Y.-L. Xie, Y.-X. Wang, H.-Y. Wu, Y.-Y. Yang and Z.-Y. Zhang, *Electrochim. Acta*, 2009, **54**, 2737.
5. M. Shao, F. Ning, Y. Zhao, J. Zhao, M. Wei, D. G. Evans and X. Duan, *Chem. Mater.*, 2012, **24**, 1192.
6. M. Shao, R. Zhang, Z. Li, M. Wei, D. G. Evans and X. Duan, *Chem. Commun.*, 2015, **51**, 15880.
7. A. Corma, V. Fornés, R. M. Martín-Aranda and F. Rey, *J. Catal.*, 1992, **134**, 58.
8. S. Ueno, K. Yoshida, K. Ebitani and K. Kaneda, *Chem. Commun.*, 1998, 295.
9. K. K. Rao, M. Gravelle, J. S. Valente and F. Figueras, *J. Catal.*, 1998, **173**, 115.
10. J. I. Di Cosimo, V. K. Díez, M. Xu, E. Iglesia and C. R. Apesteguía, *J. Catal.*, 1998, **178**, 499.
11. B. M. Choudary, M. Lakshmi Kantam, C. R. Venkat Reddy, K. Koteswara Rao and F. Figueras, *J. Mol. Catal. A: Chem.*, 1999, **146**, 279.
12. X. Duan and D. G. Evans, *Layered double hydroxides*, Springer, New York, NY; London, 2005.
13. S. Miyata, *Clays Clay Miner.*, 1975, **23**, 369.
14. F. Cavani, F. Trifirò and A. Vaccari, *Catal. Today*, 1991, **11**, 173.
15. H. Zhao and G. F. Vance, *J. Chem. Soc., Dalton Trans.*, 1997, 1961.
16. A. I. Khan and D. O'Hare, *J. Mater. Chem.*, 2002, **12**, 3191.
17. H. Nakayama, N. Wada and M. Tsuhako, *Int. J. Pharm.*, 2004, **269**, 469.
18. X. Huo, C. Dai, S. Li and X. Li, *RSC Adv.*, 2015, **5**, 8689.
19. H. Zhang, D. Pan, K. Zou, J. He and X. Duan, *J. Mater. Chem.*, 2009, **19**, 3069.
20. H. Zhang, D. Pan and X. Duan, *J. Phys. Chem. C*, 2009, **113**, 12140.
21. L. Lv, J. He, M. Wei, D. G. Evans and X. Duan, *J. Hazard. Mater.*, 2006, **133**, 119.
22. K.-H. Goh, T.-T. Lim and Z. Dong, *Water Res.*, 2008, **42**, 1343.
23. C. Chen, P. Wang, T.-T. Lim, L. Liu, S. Liu and R. Xu, *J. Mater. Chem. A*, 2013, **1**, 3877.
24. K. Zargoosh, S. Kondori, M. Dinari and S. Mallakpour, *Ind. Eng. Chem. Res.*, 2015, **54**, 1093.
25. H. A. Prescott, Z.-J. Li, E. Kemnitz, A. Trunschke, J. Deutsch, H. Lieske and A. Auroux, *J. Catal.*, 2005, **234**, 119.
26. F. Basile, G. Fornasari, E. Poluzzi and A. Vaccari, *Appl. Clay Sci.*, 1998, **13**, 329.
27. N. Kakiuchi, Y. Maeda, T. Nishimura and S. Uemura, *J. Org. Chem.*, 2001, **66**, 6620.
28. J. Feng, Y. He, Y. Liu, Y. Du and D. Li, *Chem. Soc. Rev.*, 2015, **44**, 5291.
29. D. G. Cantrell, L. J. Gillie, A. F. Lee and K. Wilson, *Appl. Catal., A*, 2005, **287**, 183.
30. V. Volli and M. K. Purkait, *Clean Technol. Environ. Policy*, 2015, **18**, 529.
31. C. C. C. M. Silva, N. F. P. Ribeiro, M. M. V. M. Souza and D. A. G. Aranda, *Fuel Process. Technol.*, 2010, **91**, 205.
32. A. V. Besserguenev, A. M. Fogg, R. J. Francis, S. J. Price, D. O'Hare, V. P. Isupov and B. P. Tolochko, *Chem. Mater.*, 1997, **9**, 241.
33. P. J. Sideris, U. G. Nielsen, Z. Gan and C. P. Grey, *Science*, 2008, **321**, 113.
34. M.-Q. Zhao, Q. Zhang, W. Zhang, J.-Q. Huang, Y. Zhang, D. S. Su and F. Wei, *J. Am. Chem. Soc.*, 2010, **132**, 14739.
35. J. Wang, G. Fan, H. Wang and F. Li, *Ind. Eng. Chem. Res.*, 2011, **50**, 13717.
36. A. Malak-Polaczyk, C. Vix-Guterl and E. Frackowiak, *Energ. Fuels*, 2010, **24**, 3346.
37. Y. Tao, L. Zaijun, L. Ruiyi, N. Qi, K. Hui, N. Yulian and L. Junkang, *J. Mater. Chem.*, 2012, **22**, 23587.
38. S. He, Z. An, M. Wei, D. G. Evans and X. Duan, *Chem. Commun.*, 2013, **49**, 5912.
39. K. L. Erickson, T. E. Bostrom and R. L. Frost, *Mater. Lett.*, 2005, **59**, 226.
40. X. Zhao, F. Zhang, S. Xu, D. G. Evans and X. Duan, *Chem. Mater.*, 2010, **22**, 3933.
41. J. Shen, M. Tu and C. Hu, *J. Solid State Chem.*, 1998, **137**, 295.
42. A. J. Marchi and C. R. Apesteguía, *Appl. Clay Sci.*, 1998, **13**, 35.
43. K. Liu, Z. Yao and Y.-F. Song, *Ind. Eng. Chem. Res.*, 2015, **54**, 9133.
44. Q. Wang, X. Zhang, J. Zhu, Z. Guo and D. O'Hare, *Chem. Commun.*, 2012, **48**, 7450.
45. Q. Wang and D. O'Hare, *Chem. Commun.*, 2013, **49**, 6301.
46. C. P. Chen, M. S. Yang, Q. Wang, J. C. Buffet and D. O'Hare, *J. Mater. Chem. A*, 2014, **2**, 15102.
47. X. Ji, W. Zhang, L. Shan, Y. Tian and J. Liu, *Sci. Rep.*, 2015, **5**, 18367.
48. (a) C. Chen, R. Felton, J.-C. Buffet and D. O'Hare, *Chem. Commun.*, 2015, **51**, 3462. (b) C. Chen, C. F. H. Byles, J.-C. Buffet, N. H. Rees, Y. Wu and D. O'Hare, *Chem. Sci.*, 2016, **7**, 1457. (c) J.-C. Buffet, C. F. H. Byles, R. Felton, C. Chen and D. O'Hare, *Chem. Commun*., 2016, **52**, 4076.
49. Y. Dou, S. Zhang, T. Pan, S. Xu, A. Zhou, M. Pu, H. Yan, J. Han, M. Wei, D. G. Evans and X. Duan, *Adv. Funct. Mater.*, 2015, **25**, 2243.
50. L. Li, Y. Feng, Y. Li, W. Zhao and J. Shi, *Angew. Chem. Int. Ed.*, 2009, **48**, 5888.
51. C. Chen, P. Gunawan and R. Xu, *J. Mater. Chem.*, 2011, **21**, 1218.
52. X. Wu, B. Li and X. Wen, *J. Nanopart. Res*, 2017, **19**, 131.
53. X. Zhang, J. Wang, R. Li, Q. Dai, R. Gao, Q. Liu and M. Zhang, *Ind. Eng. Chem. Res.*, 2013, **52**, 10152.
54. X. Liu, C. Wang, Y. Dou, A. Zhou, T. Pan, J. Han and M. Wei, *J. Mater. Chem. A*, 2014, **2**, 1682.
55. Z. Gu, J. J. Atherton and Z. P. Xu, *Chem. Commun.*, 2015, **51**, 3024.
56. D. Li, Y.-T. Zhang, M. Yu, J. Guo, D. Chaudhary and C.-C. Wang, *Biomaterials*, 2013, **34**, 7913.
57. Y. Zhao, S. He, M. Wei, D. G. Evans and X. Duan, *Chem. Commun.*, 2010, **46**, 3031.
58. M. Shao, F. Ning, J. Zhao, M. Wei, D. G. Evans and X. Duan, *J. Am. Chem. Soc.*, 2012, **134**, 1071.
59. O. Madelung, U. Rössler and M. Schulz, in *II-VI and I-VII Compounds; Semimagnetic Compounds*, Springer Berlin Heidelberg, Berlin, Heidelberg, 1999, pp. 1.

This journal is © The Royal Society of Chemistry 20xx

Please do not adjust margins